Multiscale Physical Characterization of a UV-degraded Polymeric Coating System

Xiaohong Gu, Lipiin Sung, Bouchra Kidah, Mounira Oudina, Vincent Delaurent, Haiqing Hu, Debbie Stanley, Walter E. Byrd, Jerry Y.C. Jean[1], Tinh Nguyen and Jonathan W. Martin

Materials and Construction Research Division, National Institute of Standards and Technology, Gaithersburg, MD 20899
[1]University of Missouri-Kansas City, Kansas City, MO 64110

Abstract

Surface topography and gloss are highly interdependent properties affecting the appearance of a polymeric coating system. Upon exposure to ultraviolet (UV) radiation, the surface topography of a coating becomes more pronounced and, correspondingly, its gloss normally decreases. However, the surface factors affecting gloss and appearance are difficult to ascertain. In this paper, atomic force microscopy (AFM) and laser scanning confocal microscopy (LSCM) measurements have been performed on an amine-cured epoxy coating system exposed to outdoor environments in Gaithersburg, Maryland. The formation of the protuberances is observed at the early degradation stages, followed with the appearance of circular pits as exposure continues. At long exposure times, the circular features enlarge and deepen, resulting in a rough surface topography and crack formation. Fourier Transform Infrared Spectroscopy (FTIR) study indicates that the oxidation and chain scission reactions are likely the origins of the surface morphological changes. The relationship between changes in surface roughness and gloss has been analyzed. The root mean square (RMS) roughness of the coating is related to nanoscale and microscale morphological changes in the surface of the coating as well as to the gloss retention. A near-linear dependence of RMS roughness with the measurement length scale (L) is found on a double logarithmic scale, i.e., RMS ~ L^f. The scaling factor, f, decreases with exposure time. The relationship between surface topography, on nano- to micro- scales, and the macroscale optical properties such as gloss rentention is discussed. Moreover, a recent development in using an angle-resolved light scattering technique for the measurement of the specular and off-specular reflectance of the UV exposed specimens is also demonstrated, and the optical scattering data are compared to the gloss and the roughness results.

Introduction

Polymeric coatings are commonly used to improve the appearance of buildings, bridges, aircraft and automobiles. The service life of a polymeric coating is largely controlled by how its appearance is affected by ultra-violet (UV) radiation, humidity, temperature and other aggressive weathering factors. Generally, polymeric materials degrade through photooxidation processes, such as chain scission, crosslinking, and the formation of oxidized products.[1] With prolonged exposure, these photochemical processes lead to physical and mechanical changes in a coating.[2,3] In the physical properties, the change in surface topography and gloss are two highly interdependent parameters affecting the appearance of a coated system.

The surface topography of a coating is typically measured through profiling techniques such as contact stylus instruments, phase-measuring interferometers, laser scanning confocal microscopes (LSCM) and scanning probe microscopes.[4] Contact stylus profilers are not an optimal way of measuring surface topography because they apply a force that may deform or damage the surface of the coating. Interference microscopes and confocal microscopes are non-contact measurements and, thus, they are more suitable for monitoring the coating physical changes. The capabilities of these optical microscopic techniques depend on the surface reflectivity of the coating as well as the resolution limits of the microscopes.[5] Atomic force microscopy (AFM) has become a powerful tool for quantifying the surface topography of polymeric coatings because of its 3D nanoscale resolution and the ultra low interaction force between the probe and the sample. However, AFM has limitations with respect to its maximum scanning area (usually up to 100 μm x100 μm) and the maximum measurable peak-to-valley height (usually up to 6 μm). Since surface roughness measurements strongly depend on the scanned area, we have combined AFM and LSCM to study the surface topography of a coating as a function of UV exposure. The roughness of a coating is characterized here in terms of a root mean square (RMS) roughness.

Gloss is the ratio of the intensity of the light scattered by a test surface at the angle of specular reflection compared to that from a standard specular reflecting surface under the same conditions. It is affected by both the topography of a surface and its refractive index.[5] Considerable research has been conducted to identify the relationship between RMS surface roughness and gloss.[6,7] Recent results have indicated that surface height correlations affect gloss.[8,9] The in-plane distribution of undulations on the surface of a material having correlation lengths comparable to the wavelength of the incident light must also be taken into account.[5] It is known that light scattering changes from predominately specular to predominately diffusive (off-specular) with an increase in RMS roughness.[10] Off-specular reflectances, however, are not commonly measured by commercial handheld glossmeters.

The objectives of this paper are (1) to study nanoscale-to-microscale morphological changes occurring in a UV-exposed epoxy coating, (2) to understand the relationship between the topographic changes and the gloss loss, and (3) to explore the capability of the optical scattering technique for the measurement of optical property of the degraded specimens. The topographic changes of an amine-cured epoxy are monitored by AFM and LSCM during exposure to an outdoor environmental chamber. The gloss measurement is performed using a handheld

commercial glossmeter at incident angles of both 20° and 60°. The light scattering measurements are performed on both exposed and unexposed epoxy specimens using a recently developed angle-resolved custom-designed optical scattering instrument. The relationship between surface roughness on different length scales and the gloss loss is discussed. The optical scattering data are analyzed to compare to the results from gloss and the roughness measurements.

Experimental*

Materials and Specimen Preparation

The amine-cured epoxy used in this study was a mixture of a diglycidyl ether of bisphenol A and 1,3-bis(aminomethyl)-cyclohexane (1,3 BAC) at the stoichiometric ratio. Small amounts of toluene were added to the mixture of epoxy resin and amine curing agent and the resulting mixture was stirred mechanically. After degassing in a vacuum oven to remove bubbles, the mixture of epoxy, amine and solvent was applied onto substrates in a CO_2-free, dry air glove box. Films having a thickness of approximately 150 μm were obtained by casting the mixture onto silicon wafers using a drawdown technique. All samples were cured at room temperature for 24 h in the glove box, followed by heating at 130 °C for 2 h in an air-circulating oven.

Outdoor UV Exposure

Outdoor exposures were conducted on the roof of a NIST research laboratory located in Gaithersburg, Maryland, from October 2003 through December 2005. Specimens were loaded in the multiple-window exposure cells and placed in an outdoor environmental chamber at 5° from the horizontal plane facing south. The bottom of the chamber was made of black-anodized aluminium, the top of the chamber was covered with "borofloat" glass; all four sides of the chamber were perforated and these perforations were covered with a non-moisture absorbing fabric material that acted as a filter to prevent dust particles from entering the chamber. The exposure cells were equipped with thermocouples and relative humidity (RH) sensors, and the temperature and the RH in the chamber were recorded at one minute intervals throughout the day.

Sample exposures were begun in the beginning of the month in five different months. The rates of degradation for the epoxy films exposed at each starting date differed; hence, the exposure durations required to achieve the same amount of degradation depended on the starting date. The starting months were March, July, September, October and December, and the exposures for each starting date are referred to in this paper as the March Group, the July Group, the September Group, the October Group and the December Group.

Laser scanning confocal microscopy (LSCM)

A reflection laser scanning confocal microscope (LSCM) was employed to characterize the surface morphology (topographic profile) of the specimens. A detailed description of the LSCM measurements can be found elsewhere. [3,11] The laser wavelength was 543 nm. The LSCM images are 2D intensity projections with 512 pixels by 512 pixels. The 2D intensity projection image is effectively the sum of all the light scattered by different planar layers of the coating. The

* Instruments and materials are identified in this paper to describe the experiments. In no case does such identification imply recommendation or endorsement by the National Institute of Standards and Technology (NIST).

pixel intensity level represents the amount of light scattered into the microscope objective. Darker areas represent regions that scatter less light than lighter colored regions do.

The root mean square (RMS) surface roughness S_q is calculated using a surface tilt correlation (automatic plane fit) without a numerical filter, according to the following formula:

$$S_q = \sqrt{\frac{1}{N_x \cdot N_y} \cdot \sum_{i=1}^{N_x} \cdot \sum_{j=1}^{N_y} \cdot \left[z(x_i, y_j) - S_c \right]^2} \qquad (1)$$

$$S_c = \frac{1}{N_x \cdot N_y} \cdot \sum_{i=1}^{N_x} \cdot \sum_{j=1}^{N_y} \cdot z(x_i, y_j) \qquad (2)$$

where N_x, N_y are the numbers of pixels in the *X*- and *Y*- directions, respectively.

The estimated uncertainties in the roughness data presented in this paper are plus and minus one standard deviation from the mean measurements. Roughness measurements were made at 5 different locations on each sample. All uncertainties are indicated in the figures as well as in the table. Successive LSCM measurements were performed at almost the same location on a specimen to facilitate the study of morphological changes occurring in the films as a function of UV exposure.

Atomic Force Microscopy (AFM)

A Dimension 3100 AFM (Veeco Metrology) was used to image the morphology and the microstructure of the amine-cured epoxy coatings. The AFM was operated in the tapping mode using commercial silicon probes (TESP 70, Veeco Metrology). A resonance frequency of approximately 300 kHz and a free-oscillation amplitude of 62 nm ± 2 nm were used. The set-point ratio (the ratio of set point amplitude to the free amplitude) ranged from 0.60 to 0.80. Similar to LSCM measurements, successive AFM measurements were performed at essentially the same location on a specimen to facilitate the study of morphological changes occurring in the films as a function of UV exposure.

Gloss Measurement

Gloss measurements were conducted using a handheld commercial glossmeter. The samples, which were 36 mm in diameter, were periodically removed from the exposure cells for measurement. Once removed from the exposure cell, the sample was cleaned with a dry nitrogen spray, and then 20° and 60° gloss measurements were performed. The reflection areas for 20° and 60° gloss measurements were 9 mm × 9 mm and 9 mm × 18 mm, respectively. The collection angle was ± 0.9° from the specular angle. Each sample was rotated about 45° after each measurement. A total of 8 to 10 measurements were made on each specimen at each inspection. The data presented are the average of the measurements.

Optical Scattering Measurement

To ascertain the specular and off-specular scattering distribution from the coating and the substrate surfaces, light scattering measurements were performed on both exposed and unexposed epoxy specimens using a custom-designed optical scattering instrument in the

Building and Fire Research Laboratory at NIST. The instrument consists of a laser light source, a five-axis goniometric sample stage, and a two-dimensional detector mounted in a concentric ring around the sample stage. The incident laser wavelength was 633 nm, and the beam was polarized and focused on the sample with a diameter of 400 μm. Figure 1(a) presents the optical geometry, where θ_o and θ_s are the incidence and scattering angles measured with respect to the normal of the sample, and θ_{as} is the angle measured away from the specular direction. Figure 1b shows examples of the 2D scattering profiles at different aspecular angles with respect to the incidence angle of 20°. All 2D scattering profiles presented in the paper were obtained as the center of 2D detector located 3^o away from the specular direction, i.e. $\theta_{as} = 3^o$. The results were compared to the gloss and LSCM results. The estimated uncertainties in the light scattering intensity data are to be around 4 %.

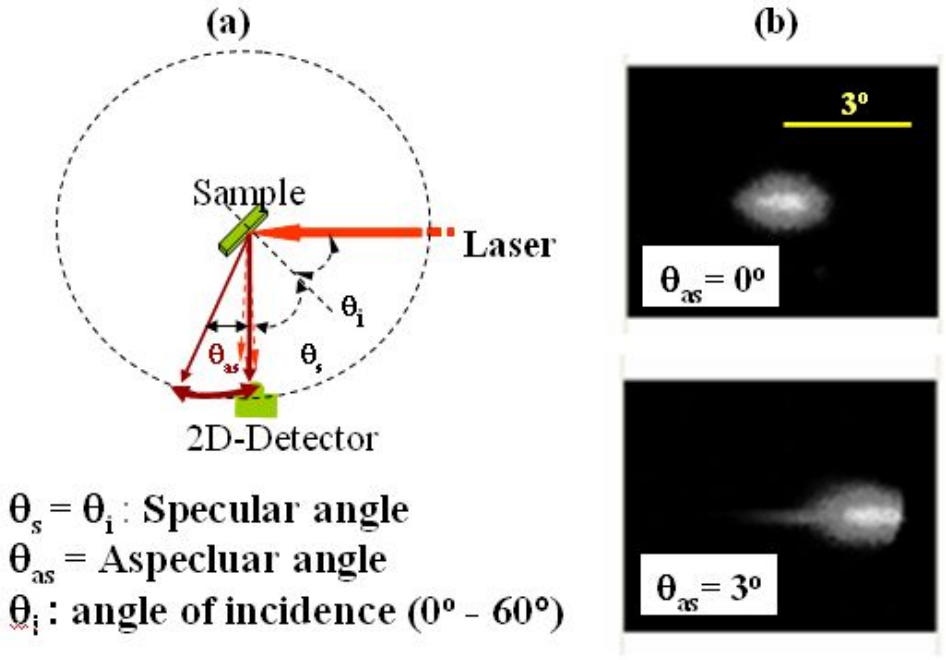

Figure 1. (a) Optical geometry of the scattering experiment, and (b) 2D scattering profile obtained from a surface at $\theta_{as} = 0^o$, and 3^o, where θ_i is the incident angle, θ_s is the specular angle, and θ_{as} is the angle measured away from the specular direction.

Fourier Transform Infrared Spectroscopy (FTIR)

Chemical degradation of the epoxy coatings was measured by FTIR transmission using a PIKE auto-sampling accessory (PIKE Technologies), described previously.[12] This automated sampling device allowed efficient and rapid recording of the FTIR transmission spectra of the coating at all windows of the exposure cell before or after each exposure time. Since the exposure cell was mounted precisely on the auto-sampler, errors due to variation of sampling at different exposure times were essentially eliminated. The auto-sampler accessory was placed in a FTIR spectrometer compartment equipped with a liquid nitrogen-cooled mercury cadmium telluride (MCT) detector. Spectra were recorded at a resolution of 4 cm^{-1} and 128 scans. The peak height was used to represent IR intensity, which is expressed in absorbance. All FTIR results were the average of four specimens.

Results and Discussion

Nanoscale Topographic Characterization with AFM

AFM topographic images of the epoxy coating after outdoor exposure in an environmental chamber located in Gaithersburg, Maryland, for a March Group specimen are shown in Figure 2. From left to right, the exposure times are (6, 38, 69, 77, and 84) d, respectively. For each row, starting from the top to the bottom, the scanning areas are 80 μm × 80 μm, 50 μm × 50 μm, 25 μm × 25 μm, 10 μm × 10 μm and 5 μm × 5 μm, respectively. Figure3 shows the 3D AFM topographic images corresponding to the 5 μm × 5 μm scan area. Approximately the same region of the sample was scanned in successive images at each scan size. General micro-scale morphological changes during degradation can be observed in the 80 μm length scan, while nanoscale structural changes are more easily observed at higher

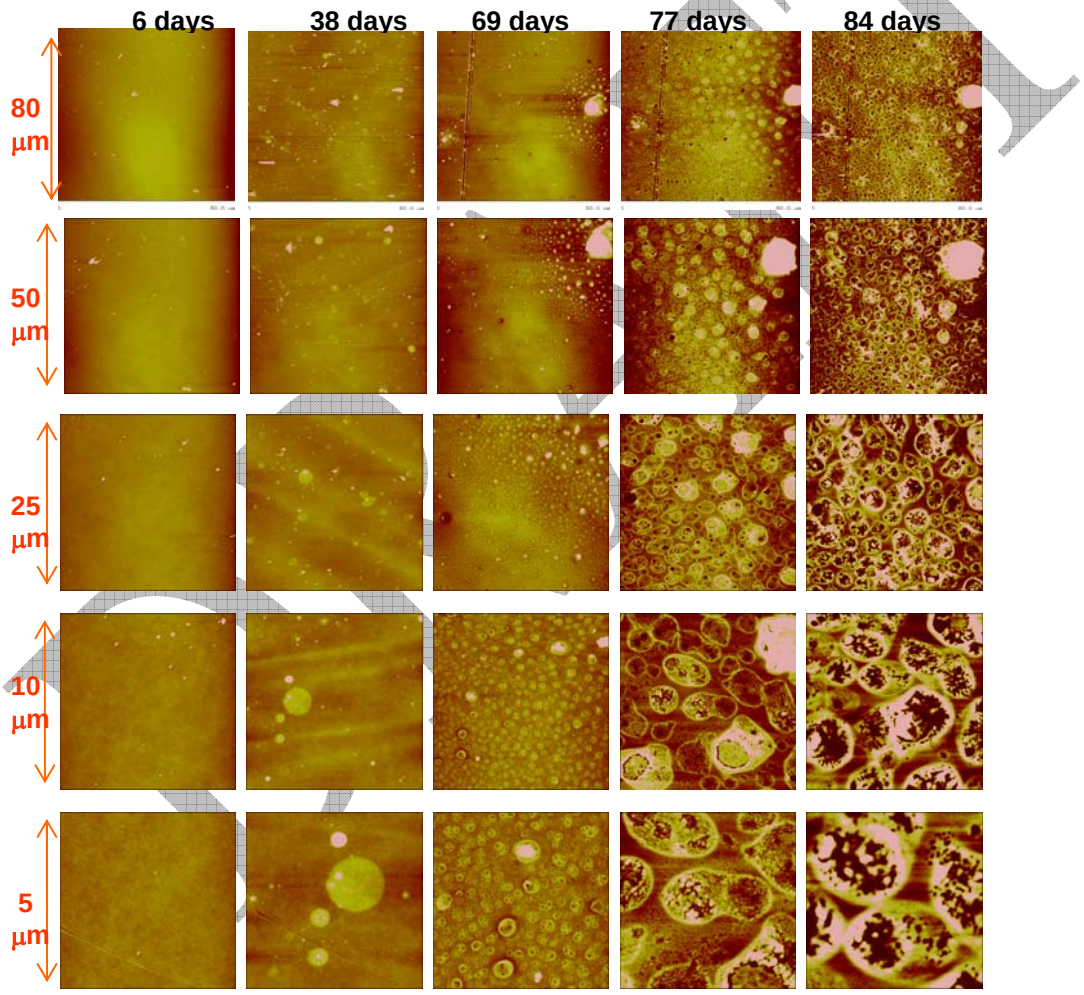

Figure 2. AFM topographic images of a March Group epoxy coating after outdoor exposure in Gaithersburg, Maryland, for (6, 38, 69, 77, 84) d, respectively from left to right. Lateral dimensions for each row of images (from top to bottom) are 80 μm, 50 μm, 25 μm, 10 μm and 5 μm, respectively.

magnifications. For the first 6 d of exposure, the surface appears to be similar to that of the unexposed samples. The small protuberances (bright spots) in these micrographs were most likely created during sample preparation. After 38 d, a few circular features are apparent, which can be seen clearly in the 10 μm or smaller scan sizes. The 3D images show that these circular features are protuberances of various sizes. After 69 d of exposure, a pronounced structure appears on the surface, surrounded by many new circular features. At higher magnifications and 3D presentation (Figure 3C), these features are identified as being pits having elevated edges and an average diameter of 0.3 μm. These pits grow in number and size such that after 77 d of exposure the entire scanned area of the specimen is covered with pits. The perimeters of these late term pits are not circular, but instead, are circularly distorted. These large pits appear to be created through the coalescence of smaller pits. The dimensions and the depth of the pits continue to increase with time such that, after 84 d of exposure, coalesced and deep pits dominate the surface topography. The elevated edges of those pits are still obvious from the micrographs. Chemical degradation processes such as oxidation, chain scission, and mass loss, are likely the major origins of these morphological changes.

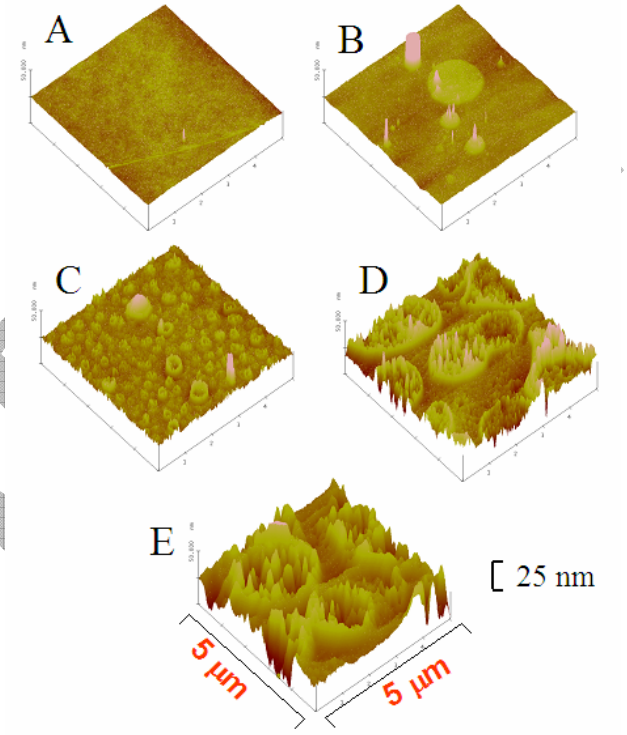

Figure 3. 3-D AFM topographic images of a March Group epoxy coating after outdoor exposure for (A) 6 d, (B) 38 d, (C) 69 d, (D) 77 d, (E) 84 d, respectively. Lateral dimensions for the images are 5 μm × 5 μm. The height scale is 25 nm.

To understand the origins of the morphological changes of the amine-cured epoxy coatings during outdoor exposure, the chemical degradation of the materials was investigated by performing the FTIR measurements on the 6 μm-thick spin-cast films on CaF_2 exposed to the same environments and from the same starting time as the March Group. Results are presented in

Figure 4. The difference spectra were obtained by subtracting the spectrum of the unexposed sample from that of the exposed one after adjusting for any baseline shift. Three exposure times close to those used in the AFM study are shown. The 1250 cm^{-1} band is attributed to C-O stretching of aryl ether, 1510 cm^{-1} to benzene ring stretching, and 2925 cm^{-1} to CH_2 anti-symmetric stretching. The decrease in intensities of these bands indicates that chain scission and mass loss in the films have taken place. In addition to the intensity decreases of the existing bands, the spectra show the formation of new chemical species in the 1620 cm^{-1} to 1800 cm^{-1} region as a result of exposures. Two prominent bands at 1658 cm^{-1} and 1728 cm^{-1}, which are assigned to C=O stretching of a ketone and amide C=O stretching, respectively, are due to formation of oxidation products. The OH stretching bands near 3400 cm^{-1} also shift to lower frequency and new bands appear around 3225 cm^{-1}. The above FTIR results are in good agreement with the photo-oxidative mechanisms proposed by Bellinger and Verdu[13,14] for epoxy cured with aliphatic amines.

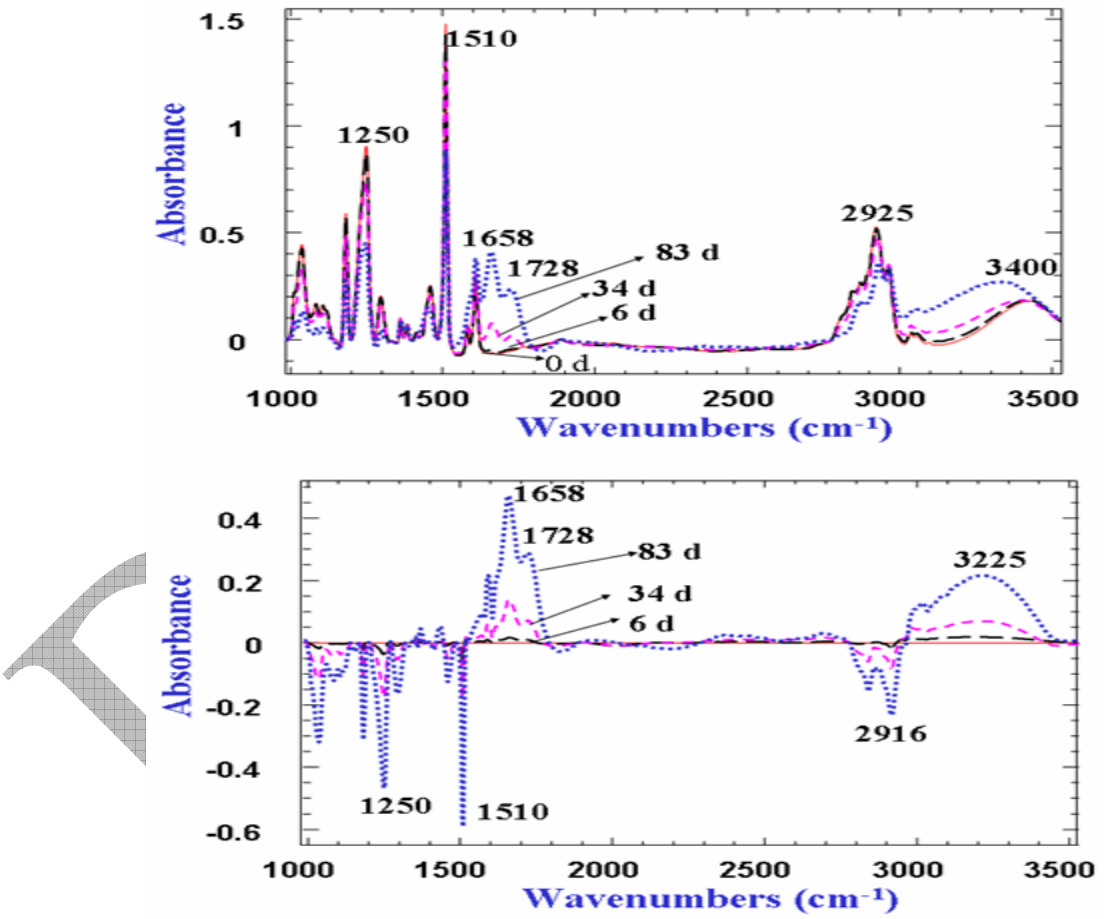

Figure 4. Plots of FTIR intensity for amide C=O stretching band (1658 cm^{-1}) and aromatic ring stretching band (1510 cm^{-1}) as a function of time of exposure to outdoors during March and June. The letters of A, B, C, D and E correspond to (6, 38, 69, 77 and 84) d of exposure, respectively. Each data point in this figure was the average of four specimens. The standard deviation of the four samples was within ± 10 % of the average value.

To establish the relationship between the nanoscale physical changes and the chemical degradation, the FTIR intensities of the amide C=O stretching band at 1658 cm^{-1} and the aromatic ring stretching band at 1510 cm^{-1} are plotted as a function of exposure time, as shown in Figure 5. The letters of A, B, C, D and E correspond to (6, 38, 69, 77 and 84) d of exposure time in the AFM study, Each data point is the average of four specimens. The standard deviation of the four samples is less than ± 10 % of the average value. The decrease in the intensity of the 1510 cm^{-1} band is nearly linear with exposure time, while the amide formation at 1658 cm^{-1} reaches a maximum after approximately 80 d and then decreases after 90 d of exposure. The nanoscale physical changes appear to follow qualitatively with chemical degradation reasonably well for the epoxy exposed to outdoors. For the first 6 d of exposure, FTIR results exhibit a small but detectable chemical changes (letter A, Figure 5). The corresponding AFM images show few visible features with low surface RMS roughness (discuss later). On further exposure, when the surface topographic changes are severe, a substantial chemical degradation has also occurred. An interesting finding is that for many groups, when the surfaces become dominated by the circular pits (similar to Figure 3D at 77 d), the amide formation (1658 cm^{-1}) is generally close to its maximum value ($\Delta A \approx 0.4$). This phenomenon does not depend on the starting time of the exposure. The results indicate that the chemical species of the circular features are probably attributed to the oxidation products, such as amide formation. Therefore, the chemical degradation processes such as oxidation and chain scission are likely the origins of the surface morphological changes observed by AFM. The cycling of the temperature and humidity, and the water condensation in the outdoor condition could also play an important role in the observed pits formation[15].

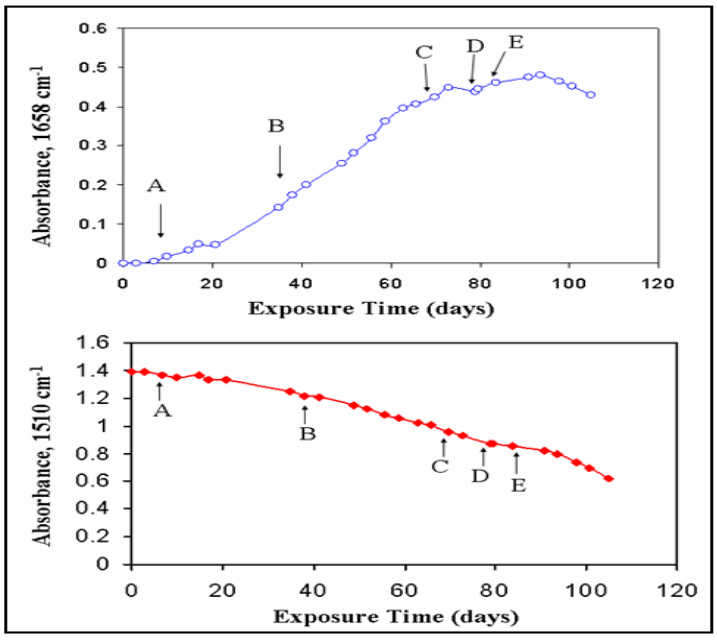

Figure 5. Plots of FTIR intensity for amide C=O stretching band (1658 cm^{-1}) and aromatic ring stretching band (1510 cm^{-1}) as a function of time of exposure to outdoors during March and June. The letters of A, B, C, D and E correspond to (6, 38, 69, 77 and 84) d of exposure,

respectively. Each data point in this figure was the average of four specimens. The standard deviation of the four samples was within ± 10 % of the average value.

LSCM Characterization and Scaling Effect on Surface Roughness

Practically, the maximum scanning area for most current AFMs is approximately 100 μm x100 μm. The estimated RMS surface roughness, however, often strongly depends on the area measured.[16] If the scanned area is too small, then the contribution that larger surface features make on the estimated RMS surface roughness is disregarded, and vice versa, i.e., if the scanning area is too large, then the contribution that small defects have on the RMS roughness may be downplayed. To circumvent this problem, the same specimens were scanned with both AFM and LCMS, and the RMS values were estimated over the range of length scales covered by these two microscopic techniques.

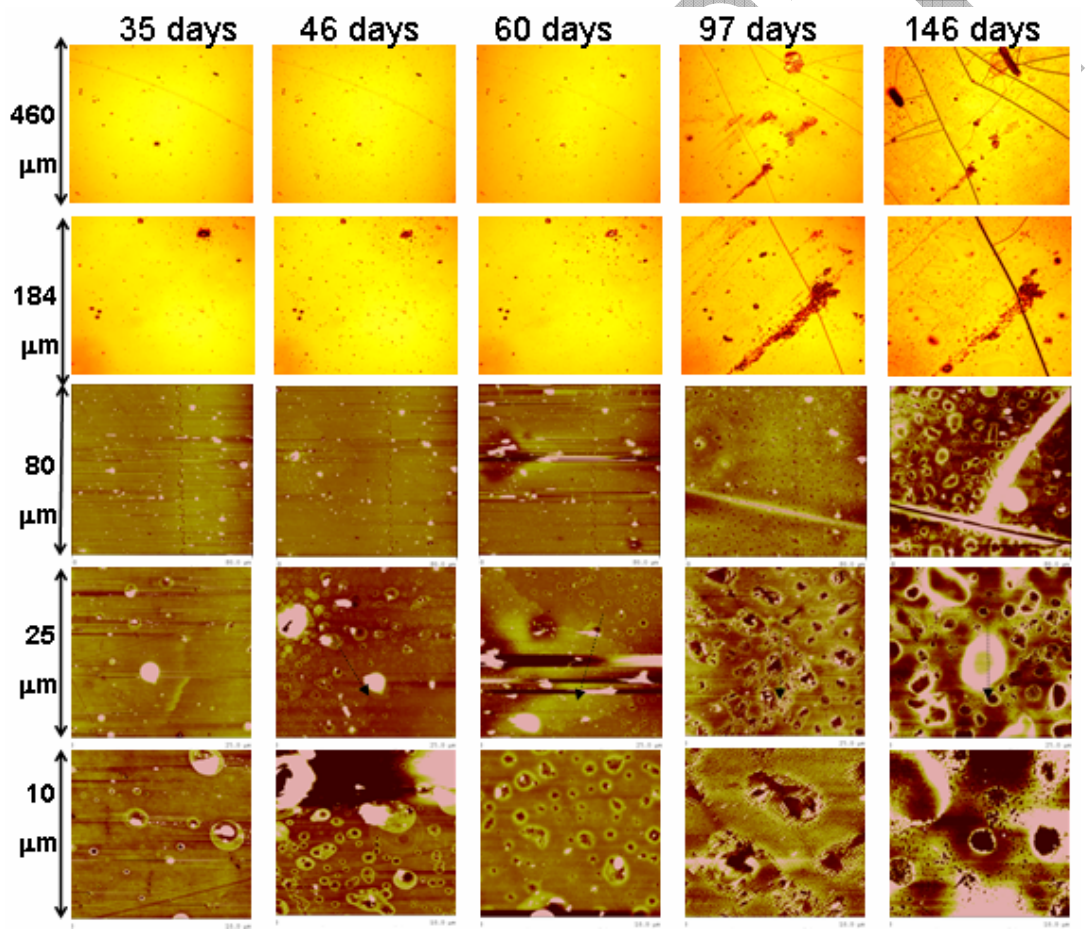

Figure 6. LSCM (top two rows) and AFM (bottom three rows) topographic images of a July Group epoxy coating after outdoor exposure in Gaithersburg, Maryland, for (from left to right) 35 d, 46 d, 60 d, 97d, 146 d and for lateral dimensions (from top to bottom) of 460 μm, 184 μm, 80 μm, 25 μm, and 10 μm, respectively.

Figure 6 shows LSCM (top two rows) and AFM images (bottom three rows) for the same July Group specimen. As expected, in Figure 6, some sub-microscale features revealed by AFM are not visible in LSCM images while the growth and the distribution of cracks, the pit density, and the large scale surface roughness that can be easily observed in the LSCM images can not be observed in the AFM. Therefore, by combining the LSCM technique with the AFM, one can obtain a global topographic perspective of the information available over a range of length scales between approximately 2 mm and a few nanometers.

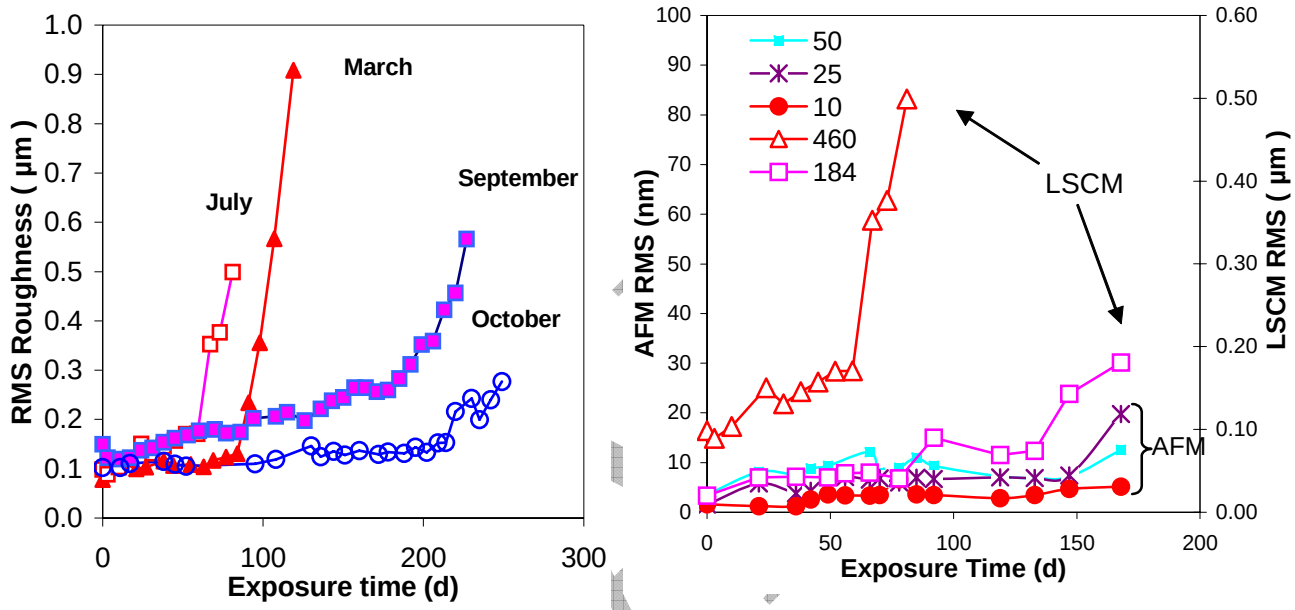

(A) (B)

Figure 7: (A) RMS roughness (LSCM) vs. exposure time for four groups with exposure starting dates in October, March, July and September. The LSCM length scale is 460 µm. The RMS data presented in each group is averaged from at least two samples; 5 different locations were measured on each sample. (B) RMS roughness vs. exposure time for different scanned sizes (July Group). The RMS roughness was obtained from the same sample using two different techniques – LSCM and AFM as indicated in the figures. The length scales are 460 µm, 184 µm, 80 µm, 25 µm, and 10 µm, respectively. Each LSCM roughness data is the average of the measurements on 5 different locations, and the AFM data is the average of 3 different locations of the same sample. Uncertainties for all data points are less than 10 %.

Further insight into topographic changes is provided by an analysis of the surface roughness. Figure 7A shows the RMS roughness as a function of exposure time for four groups exposed in the different months. These roughness values, based on 460 µm × 460 µm LSCM images, were calculated using a surface tilt correlation (automatic plane fit) without a long wavelength cutoff filter. It can be seen that the RMS roughness for all four groups increases with exposure time, though the rate of change is highly dependent on the starting month. The increasing rate of the July Group samples is the fastest, and the rate of the October Group is lowest. Differences in the power distribution of solar spectra, temperature and humidity probably lead to these differences in the roughness change rates. The effect of measurement area on the RMS roughness is shown in Figure 7B. The length scales are (10, 25 and 50) µm for the AFM

measurements, and (184 and 460) μm for the LSCM measurements. A marked dependence of surface roughness on the measurement scale is observed. For a quantitative evaluation of the measurement scale with regard to the structure characteristics of the surface, the RMS roughness values are plotted against scan sizes on a double logarithmic scale for different exposure times, as shown in Figure 8. The length scales of the measured sizes range from 2.5 μm to 460 μm. Specimens from the March and September Groups were selected for the analysis. A near-linear dependence of the RMS roughness with the measurement length scale (L) is found for the same sample in a double logarithmic scale, i.e., RMS ~ L^f. The scaling factor, f, can be obtained from the slope of the straight line. The scaling factor decreases with increasing exposure times for all groups, however, the trend of the scaling factor against exposure time varies with different groups. For example, a steeper decrease of scaling factor is found for the specimens in the March Group than for the September Group (Figure 9). These results are consistent with those reported for both fluoro-based[17] and polyurethane coatings.[18]

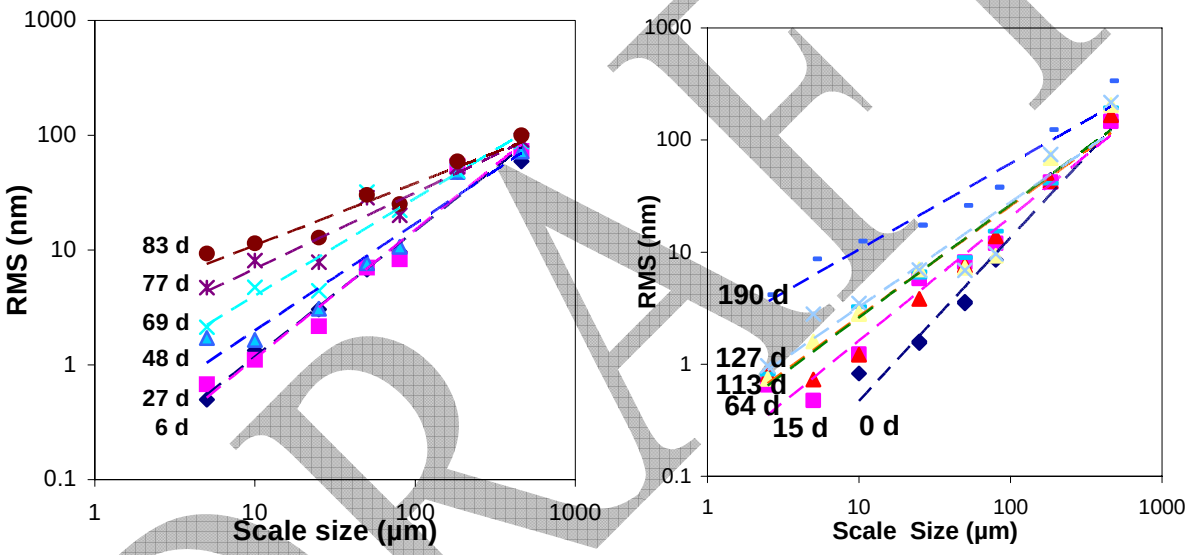

(A) (B)

Figure 8: RMS roughness vs. scan sizes on a double logarithmic scale at different exposure times. The lateral dimensions are (2.5, 5, 10, 25, 50, and 80) μm for AFM and (184 and 460) μm for LSCM. (A) and (B) represent the March group and September group, respectively. The exposure times are shown in the figures. Each LSCM roughness data is the average of the measurements on 5 different locations, and the AFM data is the average on 3 different locations of the same sample.

A linear relationship between the log of the RMS roughness and the log of the measured size has been described as a characteristic feature of a surface that has a fractal dimension.[19, 20] We believe that more sophisticated analyses, e.g., multi-scale analysis [21], power spectral density and wavelet-based method [22], need to be performed before any conclusions on the fractal character of these surfaces can be made.

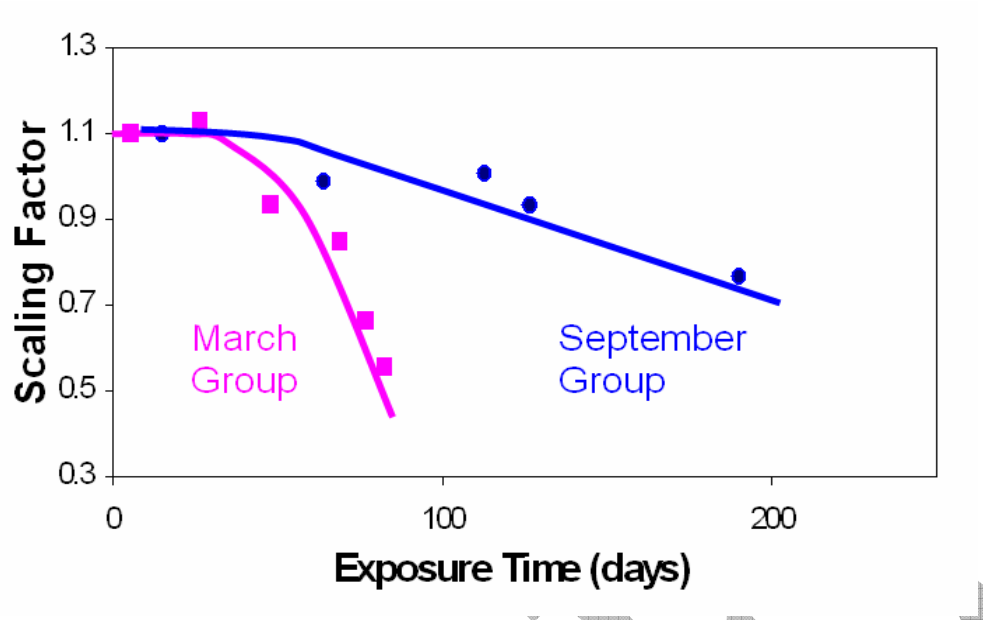

Figure 9: Scaling factor as a function of exposure time for March and September Group specimens. A faster decrease of scaling factor was found for the specimens in the March Group than for the September Group. Uncertainties for all data points are less than 10 %. Lines represent the general trend of the data.

Gloss Retention and Relationship between Optical Property and Surface Roughness

In the physical properties, the surface topography and the gloss are two highly interdependent parameters affecting the appearance of a coated system. Gloss retention is defined as the percentage change in the gloss of a specimen relative to its initial gloss value. Figures 10A and 10B show the 20° and 60° gloss retention versus the exposure time for the four exposure groups. Different groups display different gloss change behaviors, indicating that the solar power distribution, temperature, and humidity of the different seasons play a central role in the gloss loss of coating surfaces. It appears that the October Group has the longest plateau before the gloss significantly drops, while the July Group has the shortest one. Examination of the chemical changes by FTIR spectroscopy (not shown) indicate that the photo-oxidation and chain scission between the different groups have a similar trend to the physical changes, i.e., the July group changes fastest while the October group changes slowest.

Figure 11 shows the correlation between roughness and gloss retention in the early stages of the degradation of the September Group for two scan sizes: (A) 50 μm × 50 μm by AFM, and (B) 460 μm × 460 μm by LSCM. For both length scales, the estimated correlation coefficient between the gloss retention and RMS roughness is slightly higher for 60° gloss than 20° gloss measurements ($R^2 = 0.82$ *vs* $R^2 = 0.78$ for the 50 μm scan size, and $R^2 = 0.93$ *vs.* $R^2 = 0.87$ for the 460 μm scan size, where R is the correlation coefficient). As discussed previously, gloss measurement by a commercial handheld glossmeter only collects a narrow angular range of light scattered around the specular direction. With the increase of RMS roughness, the proportion of the specular scattering in the total light scattering profile decreases.[9] For rougher surfaces, the 60° gloss measurement provides a higher signal to noise than the 20° gloss measurement due to a

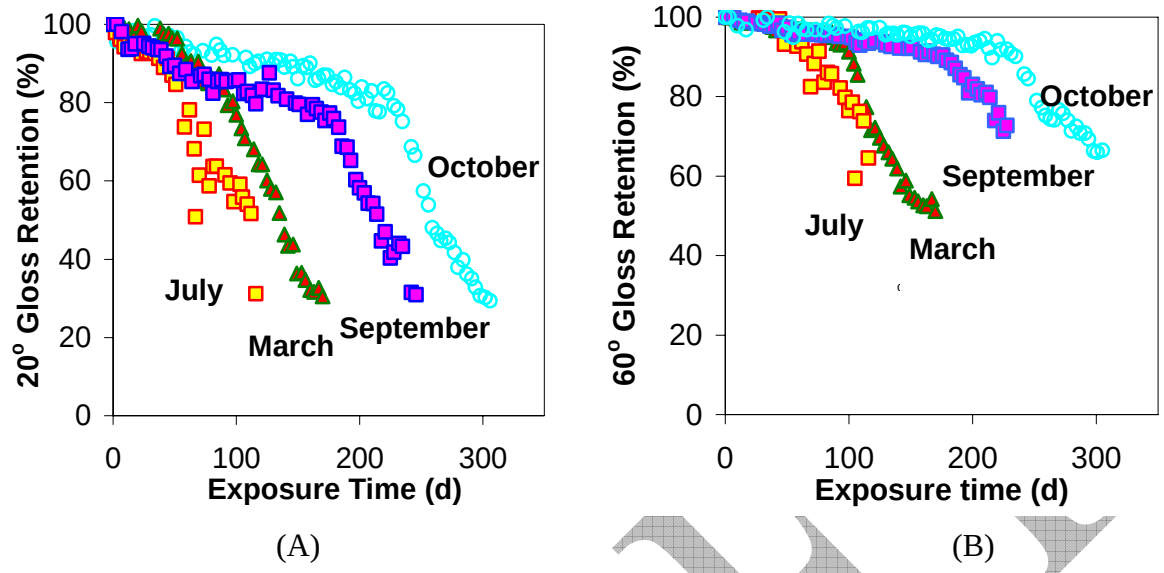

(A) (B)

Figure 10: (A) 20° and (B) 60° gloss retention vs. exposure time for four groups, which were exposed starting in October, March, July and September, respectively. 60° gloss retention changes tend to lag behind the 20° gloss retention changes. The gloss data is the average of 8 to 10 measurements on each specimen. Variations for all data points are less than 10 %.

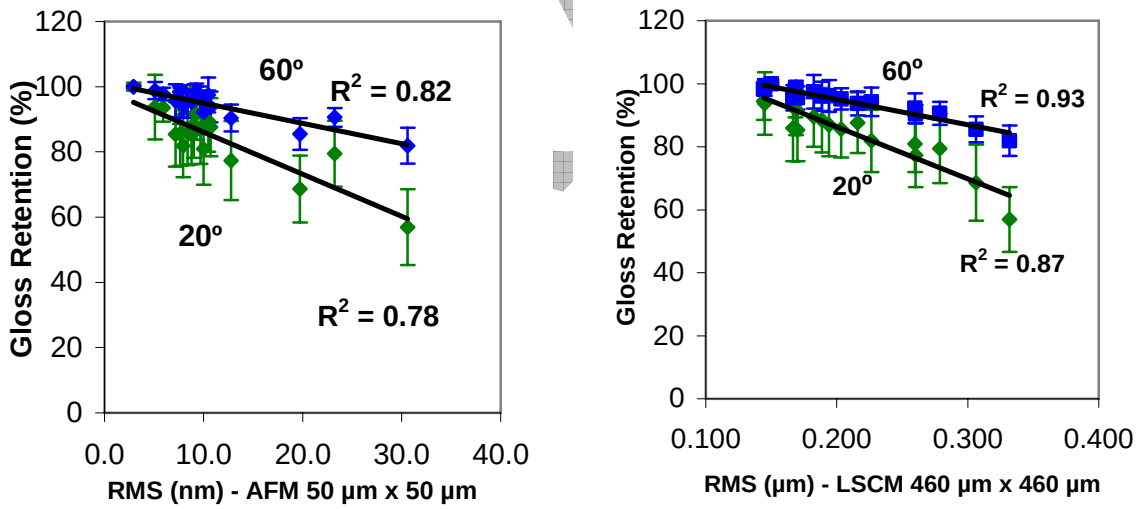

(A) (B)

Figure 11: Correlation between roughness and gloss retention for two scan areas for September Group: (A) 50 µm × 50 µm by AFM, and (B) 460 µm × 460 µm by LSCM. R is the correlation coefficient. The uncertainty bars represent one-standard deviation.

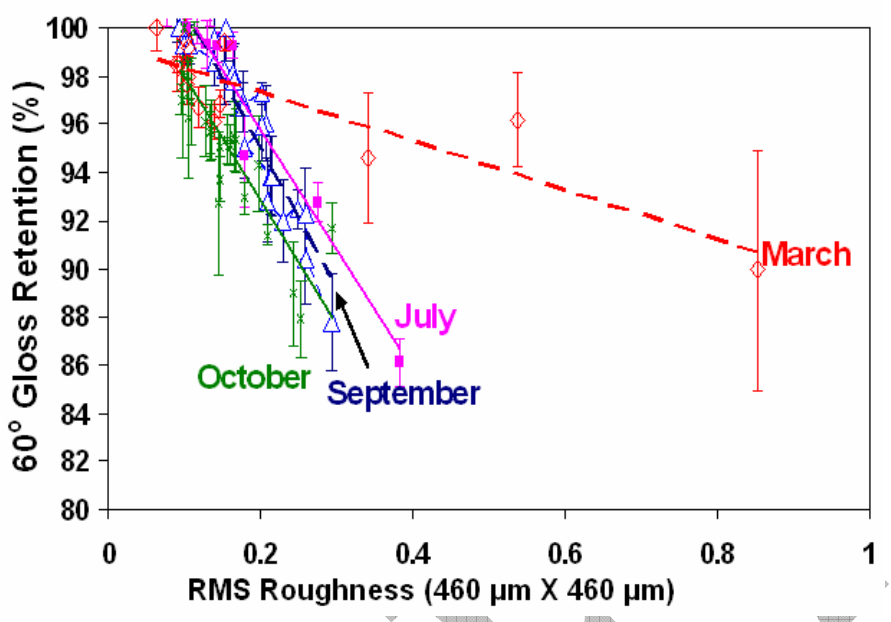

Figure 12: 60° Gloss retention vs. RMS roughness for four groups, which were exposed starting in October, March, July and September, respectively. The slope of the March Group specimens is significantly different from the slopes of the July, September, and October Groups. The uncertainty bars represent one-standard deviation.

higher reflectance values for incident angle of 60° than that of 20°.[9] Additionally, the correlation coefficient between the gloss retention and RMS roughness is slightly higher for the RMS obtained from the 460 µm × 460 µm scan area than those from the 50 µm × 50 µm scan area (R^2: 0.93 *vs.* 0.82 for 60° and 0.87 *vs.* 0.78 for 20°). Similar results have been reported from other AFM and LSCM studies on the weathering of polymeric coatings.[21,23,24] These observations indicate that while higher magnification images are very important for visualizing physical changes occurring in the very early stage of coating degradation[22,25], the longer wavelength surface roughness may be more directly related to the gloss measurement. More quantitative analysis can be provided by mathematical models.[8]

As mentioned previously, the selected four groups exhibit an increase in the RMS roughness (Figure 7) and a corresponding decrease in the gloss retention (Figure 10) with longer outdoor exposure. To further establish the relationship between gloss and the roughness, 60° gloss retention of these four groups is plotted against the RMS roughness obtained from 460 µm × 460 µm measured areas (Figure 12). All groups exhibit a linear relationship ($R^2 \approx 0.90$) between the gloss retention and the RMS roughness, though the March Group shows a significantly different slope from the other groups. These results indicate that a qualitative relationship between microscale topographical changes and macroscale appearance could be established.

However, as seen in the plots of Figure 12, groups having similar RMS values can have substantially different gloss retentions. This represents a shortcoming in the use of RMS alone to represent the roughness of a surface. Since the RMS roughness does not take the distance between surface features into account, a surface with a few distantly spaced high-amplitude features may have the same RMS value as one with many closely spaced low-lying features[5], which is suggested by the images in Figure 13A. On the other hand, specimens having similar

gloss values may have significantly different roughness (Figure 13B), indicating the deficiency in using specular reflectance alone to describe the appearance of a surface.

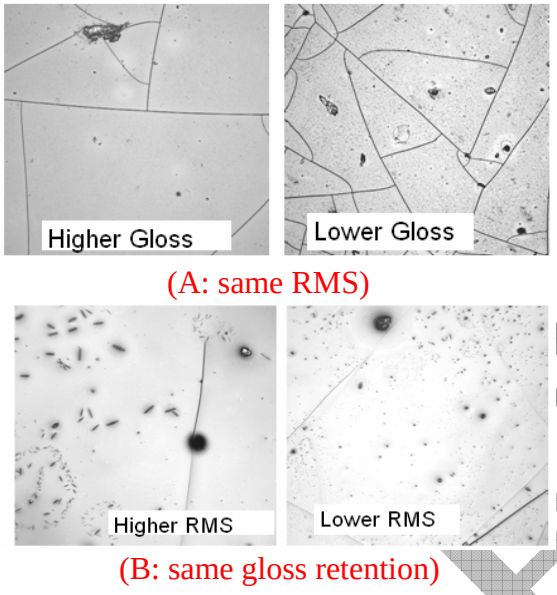

Figure 13: LSCM images of (A) two exposed samples with same RMS value but different gloss retention (RMS=0.385 μm, and 20° gloss retention are 88 % for left image and 80 % for right image); and (b) two exposed samples with same gloss but different RMS values (20° gloss retention is 90 %, and RMS=0.407 μm for left image and 0.193μm for right image).

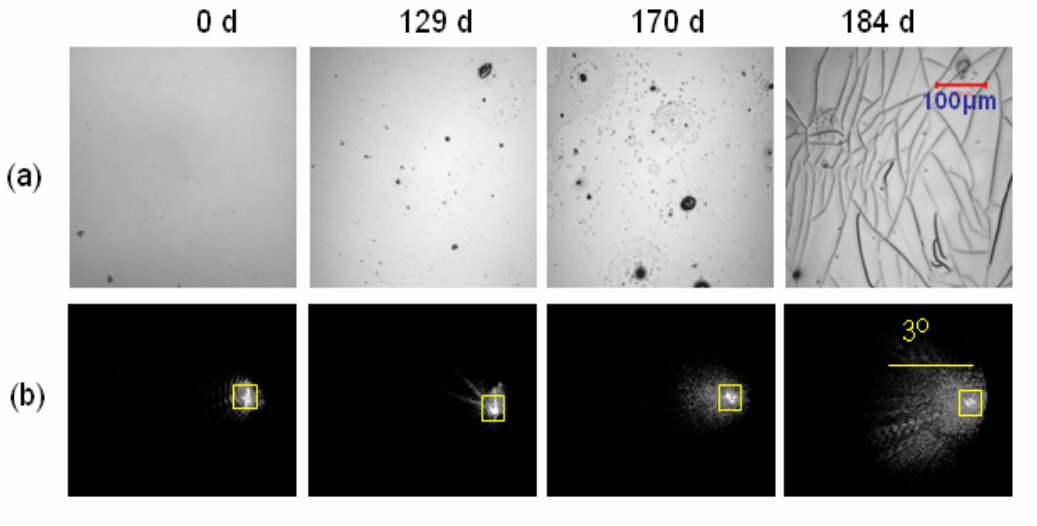

Figure 14. (a) 2D projection LSCM images of a December Group epoxy coating after outdoor exposure for (from left to right) 0 d, 129 d, 170 d and184 d; (b) the corresponding 2D optical scattering profiles for incident angle of 20° with a aspecular angle of 3°. The box in the scattering profiles is the specular region, equivalent to the specular gloss measurement by commercial glossmeter.

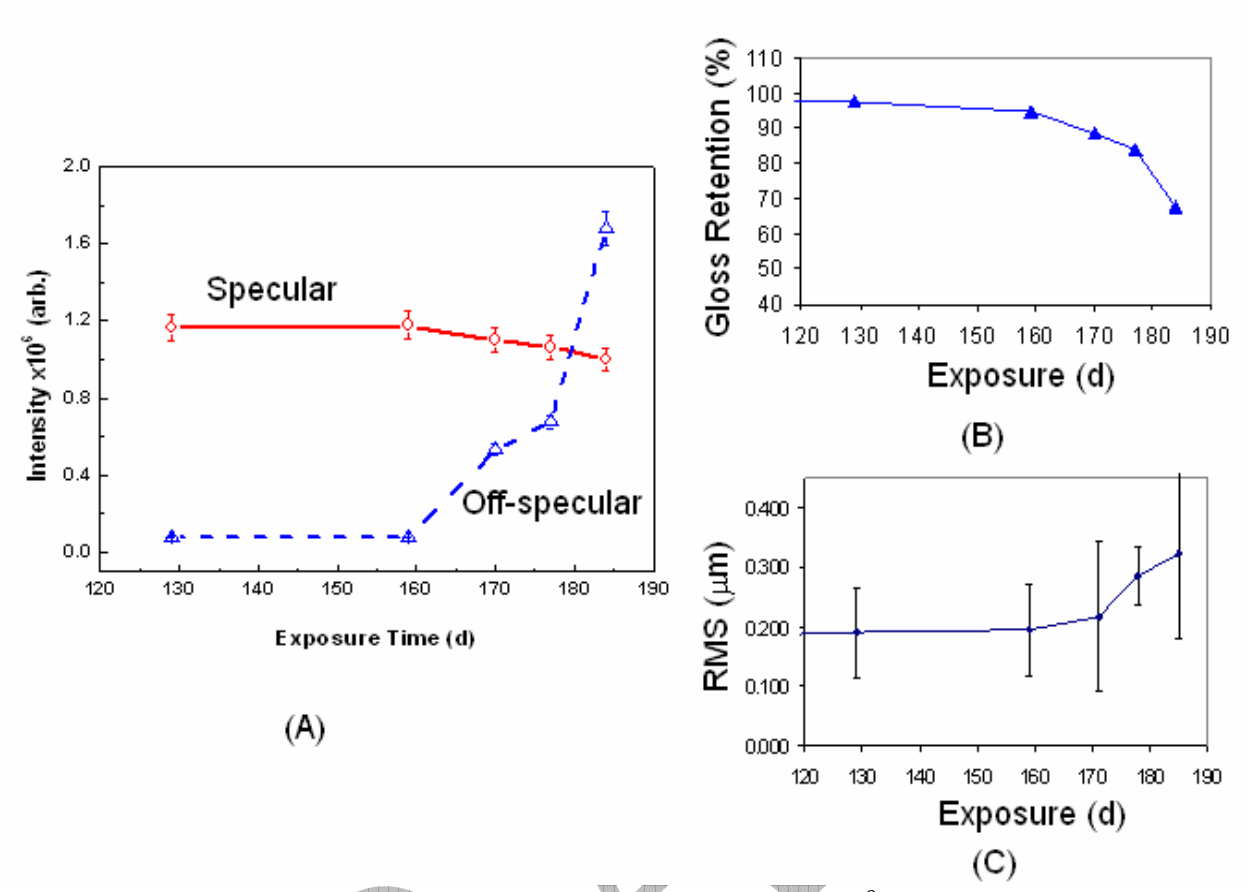

Figure 15. (A) Optical scattering intensity vs. exposure time, (B) 20° Gloss retention (%) vs. exposure time, and (C) LSCM RMS roughness vs. exposure time for a December Group exposed to outdoors.

Recently, we have developed a metrology to use the angle-resolved light scattering technique for the measurement of the specular and off-specular reflectance of the UV exposed specimens. The results are used to compare to the results from the gloss and the roughness measurements. Figure 14 displays LSCM images of a December Group specimen after outdoor exposure for different times, along with their corresponding 2D optical scattering profiles. Quantitatively, the scattering intensities of the specular reflectance and off-specular diffusive scattering were plotted against the exposure time (Figure 15A). As can be seen, the specular intensity decreases with the increase in the exposure time, which is consistent with the change of the gloss retention shown in Figure 15B. On the other hand, the intensity of the off-specular reflectance increases dramatically, overpassing the intensity of the specular reflectance at 179 days of exposure. The general trend of the off-specular scattering is similar to the change of the RMS roughness (Figure 15C). It suggests that the major contribution of the off-specular scattering is probably from the surface roughness given the subsurface structures do not change. These preliminary results indicate that the commercial gloss measurement may not fully describe a rough surface when off-specular scattering becomes significant. Future work includes applying an optical scattering model[26] to the AFM and LSCM profile data, and then the correlation between the nanoscale/microscale topographical changes and macroscale appearance can be predicted.

Summary

AFM and LSCM techniques have been used to characterize the nanoscale and microscale topographical changes of an amine-cured epoxy coating exposed to outdoors at different starting times, and the relationship between surface roughness changes and gloss loss has been analyzed. The formation of the spotty protuberances is observed by AFM at the early degradation stages, followed with the appearance of circular pits as exposure continues. At long exposure times, the circular features enlarge and deepen, resulting in a rough surface topography and crack formation. FTIR analyses reveal that the oxidation and chain scission reactions are likely the origins of the surface morphological changes, and a qualitative correlation between nanoscale physical changes and chemical degradation is observed. The RMS roughness of the specimens from different exposure groups has been found to increase with exposure time; while the rate of change is highly dependent on the exposure starting month. The result shows a near-linear dependence of RMS with the measurement length scale on a double logarithmic scale. Further, the coefficient of correlation between gloss retention and RMS roughness is slightly higher for the 60° gloss than for the 20° gloss, and gloss of both angles appear to relate better with the roughness obtained by LSCM than that measured by AFM. Moreover, the limitations of using RMS roughness or the commercial glossmeter alone to describe the appearance of some UV exposed specimens are discussed. Recent work on the angle-resolved optical scattering measurement on the degraded epoxy coatings has shown that, when the surface roughness increases with the UV exposure time, the contribution of the off-specular scattering to the appearance of the specimens becomes more significant. It appears that the off-specular scattering is mainly from the surface roughness given the subsurface structures do not change. This preliminary study indicates that, by applying an optical scattering model to the AFM and LSCM data, the correlation between the surface morphology of the polymeric coatings and the macroscale appearance could be predicted.

ACKNOWLEDGEMENTS

This research is part of a Government/Industry consortium on Service Life Prediction of Coatings at NIST. Companies involved in this consortium include Akzo Nobel, Arkema Inc., Atlas Material Testing Technologies LLC, Dow Chemical, and Sherwin Williams. Federal Highway Administration, Wright Patterson AFB, and Forest Products Laboratory also provided additional funds for this research. We thank DOW Chemical for providing the epoxy resin, and Sherwin Williams for providing the urethane resin.

References:

1. Rabek, J. F. In Polymer Photodegradation – Mechanisms and Experimental Methods; Chapman &Hall, New York, 1995, p 4.
2. VanLandingham, M.R.; Nguyen, T.; Byrd, W.E.; Martin, J.W. J Coat Technol 2001, 73, 43.
3. Sung, L.; Jasmin, J.; Gu, X.; Nguyen, T.; Martin, J. W. J. Coat Technol Research 2004, 1 (4), 267.
4. Vorburger, T.V.; Dagata, J.A.; Wilkening, G.; Iizuka, K. In Beam Effects, Surface Topography, and Depth Profiling in Surface Analysis; Czanderna et al. Eds.; Plenum Press, New York, 1998.
5. Assender, H.; Bliznyuk, V.; Porfyrakis, K. Science, 2002, 297, 973.
6. Davies, H. In Proc. Inst. Electr. Eng. Part IV, 1954, V. 101, p. 209.
7. Beckmann, P.; Spizzichino, A. In The Scattering of Electromagnetic Waves from Rough Surfaces; Pergamon Press Ltd., London, 1987.
8. Alexander-Katz, R.; Barrera, R.G. J Polym Sci Part B: Polym Phys 1998, 36, 1321.
9. McKnight, M. E.; Marx, E.; Nadal, M.; Vorburger, T. V.; Barnes, P. Y.; Galler, M. A. Appl Optics, 2001, 40(13), 2159.
10. Bennett, J.M.; Mattsson, L. In Introduction to Surface Roughness and Scattering; Opt. Soc. Am., Washington, D.C., 1989.
11. Corle, T.R.; Kino, G.S. In Confocal Scanning Optical Microscopy and Related Imaging Systems; Academic Press, 1996, pp 37-39
12. Gu, X., Nguyen, T., Ho, D.L., Oudina, M., Martin, D., Kidah, B., Jasmin, J., Rezig, A., Sung, L., Byrd, E., Jean, Y.C., and Martin, J. W., Journal of Coatings Technology Research, 2 (7), 547 (2005).
13. Bellinger, V., and Verdu, J., "Oxidative Skeleton Breaking in Epoxy-Amine Networks," *J. Appl. Polym. Sci.*, 30, 363 (1985).
14. Bellinger, V., and Verdu, J., "Structure-Photooxidative Stability Relationship of Amine-Crosslinked Epoxies," *Polymer Photochemistry*, 5, 295-311 (1984).
15. Gu, X., Martin, D., Rezig, A., Kidah, B., Cleri, C., Stanley, D., Nguyen, T., and Martin, J.W., Proceedings of 29th Adhesion Society Meeting, 154 (2006).
16. Sayles, R.S.; Thomas, T.R. Nature, 1978, 271, 431.
17. J. Faucheu, L.P. Sung, J.W. Martin, K.A. Wood, "Relating Gloss Loss to Topographical Features of A PVDF Coating", FSCT·ICE 2004 Proceedings of the 82th Annual Meeting Technical Program, McCormick Place North, Chicago, IL, October 27-29, 2004.
18. Johnson, M.A.; Cote, P.J. J Coat Technol 2003, 75, 51.
19. Bliznyuk, V.N.; Burlakov, V.M.; Assender, H.E.; Briggs, G.A.D.; Tsukahara, Y. Macromol Symp 2001, 167, 89.
20. Mandelbrot, B.B. In The Fractal Geometry of Nature; Freeman, New York, 1982.
21. Bigerelle, M.; Gorp, A.V.; Lost, A. In Proceedings of 10th International Conference Metrology and Properties of Engineering Surfaces, 2005, pp. 69-80.
22. Jiang, X.; Blunt, L. Wear, 2004, 25, 1235.
23. Gu, X.; Nguyen, T.; Ho, D.L.; Oudina, M.; Martin, D.; Kidah, B.; Jasmin, J.; Rezig, A.; Sung, L.; Byrd, E.; Jean, Y.C.; Martin, J. W. J Coat Technol Research, 2005, 1, 547.
24. Biggs, S.; Lukey, C.A.; Spinks, G.M.; Yau, S.T. Prog Organic Coat 2001, 42, 49.

25. Gu, X.; Nguyen, T.; Sung, L.; VanLandingham, M.R.; Nguyen, D.; Fasolka, M.J.; Chang, N.; Wu, T.; Jean, Y.C.; Martin, J.W. J Coat Technol Research, 2004, 1(3), 191.
26. Hunt, F. Y.; Marx, E.; Meyer, G. W.; Vorburger, T. V.; Walker, P. A.; Westlund, H. B.In Service Life Prediction: Methodology and Metrologies; Martin, J. W.; Bauer, D. R., Eds., ACS Symposium Series 805, Oxford University press, 2002.